ADVANCED MATERIALS INTERFACES
www.advmatinterfaces.de

Multi-Element Surface Coating of Layered Ni-Rich Oxide Cathode Materials and Their Long-Term Cycling Performance in Lithium-Ion Batteries

Sören L. Dreyer, Katja R. Kretschmer, Đorđije Tripković, Andrey Mazilkin, Richard Chukwu, Raheleh Azmi, Pascal Hartmann, Matteo Bianchini, Torsten Brezesinski,* and Jürgen Janek*

The energy density of layered oxide cathode materials increases with their Ni content, while the stability decreases and degradation becomes more severe. A common strategy to mitigate or prevent degradation is the application of protective coatings on the particle surfaces. In this article, a room-temperature, liquid-phase reaction of trimethylaluminum (TMA) and tetraethyl orthosilicate (TEOS) with adsorbed moisture on either $LiNi_{0.85}Co_{0.10}Mn_{0.05}O_2$ or $LiNiO_2$, yielding a hybrid coating that shows synergetic benefits compared to coatings from TMA and TEOS individually, is reported. The surface layer is investigated in long-term pouch full-cell studies as well as by electron microscopy, X-ray photoelectron spectroscopy, and differential electrochemical mass spectrometry, demonstrating that it prevents degradation primarily by a fluorine-scavenging effect, and by reducing the extent of rock salt-type phase formation.

1. Introduction

As the use of portable electronics and the market share of electric vehicles increase, so does the demand for batteries with high energy density. The current technology of choice is the lithium-ion battery (LIB), where the specific energy strongly depends on the specific capacity of the cathode active material (CAM).[1] In general, layered oxides of the type $Li_{1+x}(Ni_{1-y-z}Co_yMn_z)_{1-x}O_2$, so-called NCM CAMs, provide the highest specific capacity in practical cells.[2] Within this materials family, the available specific capacity increases with the nickel content for a fixed cut-off voltage.[3] However, this increase comes at the price of reduced structural stability and therefore accelerated degradation during battery operation.[4,5] Such effect is especially severe for the endmember in terms of nickel content, $LiNiO_2$ (LNO).[6,7] Multiple strategies to mitigate degradation and increase capacity retention have been developed and reviewed, with doping/elemental substitution and coating being the most prominent ones.[8,9] As the application of a coating in industry is currently a post-synthesis step independent from the main high-temperature calcination of the material itself, various coating strategies and chemistries have been reported.[10,11,12] Aluminum oxide has emerged as an inexpensive, yet effective coating material, applied through a variety of methods, including atomic layer deposition (ALD), wet-chemistry, and dry coating routes with different protective mechanisms proposed.[13–17] Mechanistically, these coatings are reported to protect the CAM by scavenging HF,[13] by forming beneficial electrolyte additives in a reaction with $LiPF_6$,[14] by suppressing surface phase transformations[15] or by reducing resistance and improving lithium diffusivity.[16]

S. L. Dreyer, K. R. Kretschmer, Đ. Tripković, A. Mazilkin, R. Chukwu, P. Hartmann, M. Bianchini, T. Brezesinski, J. Janek
Battery and Electrochemistry Laboratory (BELLA)
Institute of Nanotechnology
Karlsruhe Institute of Technology (KIT)
Hermann-von-Helmholtz-Platz 1, 76344 Eggenstein-Leopoldshafen, Germany
E-mail: matteo.bianchini@uni-bayreuth.de; torsten.brezesinski@kit.edu

The ORCID identification number(s) for the author(s) of this article can be found under https://doi.org/10.1002/admi.202101100.

DOI: 10.1002/admi.202101100

Đ. Tripković, P. Hartmann, M. Bianchini
BASF SE
Carl-Bosch-Str. 38, 67056 Ludwigshafen am Rhein, Germany

A. Mazilkin
Institute of Solid State Physics
Russian Academy of Sciences
Chernogolovka 142432, Russia

R. Azmi
Institute for Applied Materials – Energy Storage Systems
Karlsruhe Institute of Technology (KIT)
Hermann-von-Helmholtz-Platz 1, 76344 Eggenstein-Leopoldshafen, Germany

J. Janek
Institute of Physical Chemistry & Center for Materials Research (ZfM/LaMa)
Justus-Liebig-University Giessen
Heinrich-Buff-Ring 17, 35392 Giessen, Germany

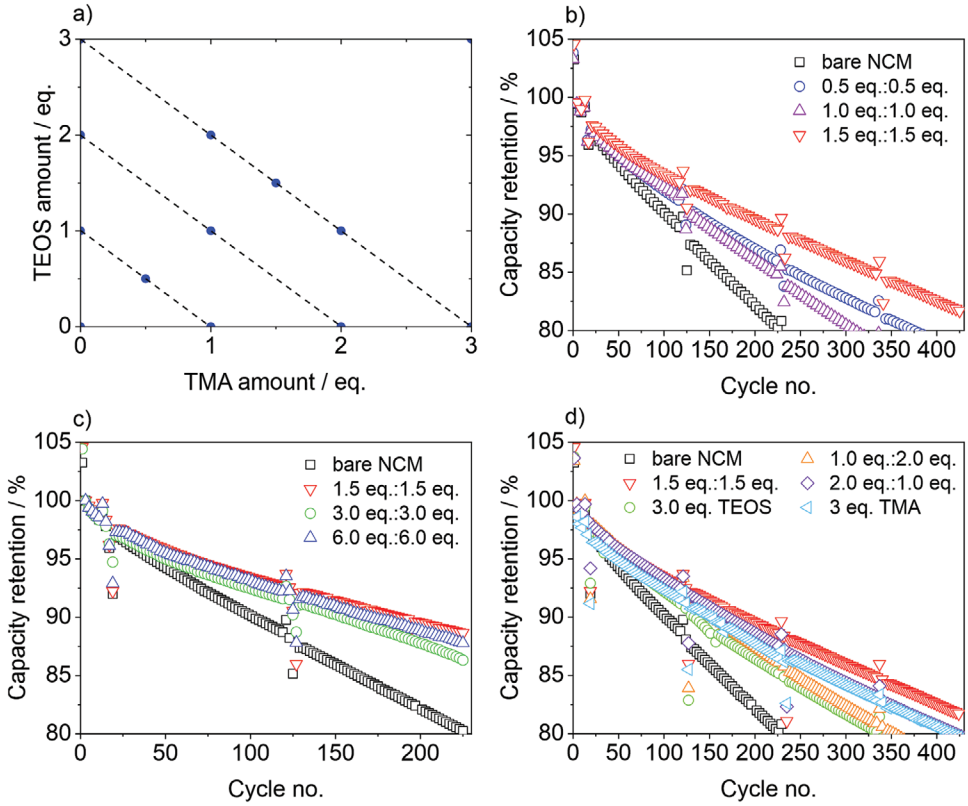

Figure 1. a) DoE-like testing of different reagent amounts and compositions. b) Performance of coated and uncoated NCM851005 CAMs in coin full cells for different total amounts of equimolar mixtures. c) Performance at higher reagent amounts. No further improvement in capacity retention is noticed after 1.5 equiv.:1.5 equiv. d) Performance of different compositions at 3 equiv. total amount. Cells tested at 45 °C, 1.0 C, 3.0–4.2 V.

In the past, we have reported a coating process that exploits the reactivity of a typical ALD precursor, trimethylaluminum (TMA), with moisture adsorbed on the CAM particle surface, almost doubling the cycle life of NCM811 (80% Ni).[18] In the present work, we show that the addition of tetraethyl orthosilicate (TEOS) as a second coating reagent yields a hybrid coating, enabling enhanced electrochemical performance of NCM851005 (85% Ni). We investigate the interplay of reagent ratio and total amount in a design of experiments (DoE)-like approach. TEOS alone leads to silica coatings for which HF scavenging, increased diffusivity, and reduced impedance are reported as mechanisms improving performance of Ni-rich NCM materials.[19–23] In a direct comparison between alumina and silica coatings, alumina has been reported to be more beneficial.[24] The combination of TMA and TEOS via ALD is known to give aluminosilicates and, in combination with a lithium precursor, has been used in electrochemical research to obtain lithiated aluminosilicate-type solid electrolytes.[25] However, a cathode coating based on this combination has, to the best of our knowledge, not yet been reported.

To further highlight the potential of our coating methodology, we then apply it to a more challenging material, namely LNO. We investigate its performance in pouch full cells, where so far only one study for LNO exists,[26] thereby broadening the spectrum of assembly and cycling conditions. Finally, the mechanism of protection on both NCM851005 and LNO is thoroughly investigated and discussed based on DEMS, electron microscopy, and XPS characterizations.

2. Results and Discussion

2.1. Coating of NCM851005 CAM

To investigate the interplay between the total reagent amount and reagents ratio, the coating was applied to NCM851005 and the electrochemical performance of the resultant materials was evaluated. **Figure 1**a summarizes the TMA:TEOS combinations used in a DoE-like grid. Note that 1 equiv. is equal to 100 µmol of coating reagent per 1 g of CAM.

Figure 1 also reports the cycling performance of the coated NCM851005 CAMs in coin cells. Figure 1b,c shows that the capacity retention achieved for different equimolar mixtures is best at a total amount of 3 equiv.. A further increase in the reagent amount to a total of 6 or 12 equiv. did not improve the capacity retention any further, likely due to increased thickness and resistance of the coating. The first-cycle specific discharge capacity for uncoated, 1.5 equiv.:1.5 equiv. and 6.0 equiv.:6.0 equiv. coated NCM851005 was 196, 192 and 183 mAh g_{CAM}^{-1}, respectively. The respective specific capacity versus cycle number curves are shown in Figure S1, Supporting Information. For aluminum oxide coatings from ALD, the optimal thickness has been reported to be just four Al_2O_3 layers.[17] These findings justify the limitation of the experimental grid in Figure 1a to a total amount of not more than 3 equiv.. Although the coating thickness was not examined directly with the DOE-like approach, it was part of the

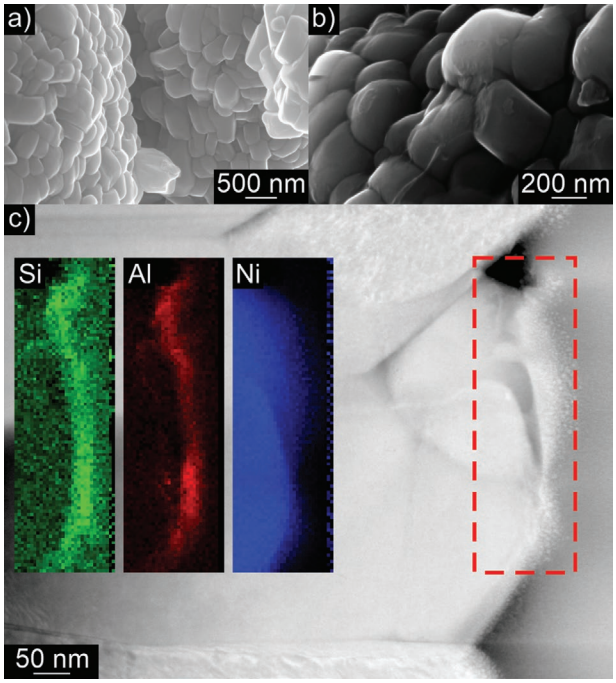

Figure 2. a,b) Surface constitution of the uncoated and coated (1.5 equiv.:1.5 equiv.) NCM851005 CAMs. c) STEM-EDS analysis of coated material showing the presence of a protective layer on the particle surface.

tailoring process, as is evident from Figure 1c and Figure S1c, Supporting Information.

The effect of varying the ratio of TMA to TEOS is shown in Figure 1d for a total amount of 3 equiv.. It was found that an equimolar ratio of TMA and TEOS gives higher capacity retention than the reagents individually or combined in a 2:1 ratio, suggesting a synergetic effect and establishing the 1.5 equiv.:1.5 equiv. mixture as the best-performing reagent mixture. This synergy is also visualized in Figures S2 and S3, Supporting Information. Taking the increased cycle life as a key metric, in the following, this optimal coating was used for a more detailed investigation.

The morphology of the coating was probed by scanning electron microscopy (SEM) (**Figure 2**a,b), SEM-energy dispersive X-ray spectroscopy (SEM-EDS; Figure S4, Supporting Information), and scanning transmission electron microscopy-EDS (STEM-EDS; Figure 2c). While SEM alone only shows the presence of rounded and bridged edges as primary indicators of the surface layer, SEM-EDS indicates a uniform coating element distribution both between and within the secondary particles and STEM-EDS reveals a ≈20 nm coating on a secondary particle. This layer thickness is different to very thin but dense ALD coatings, since with the chosen approach, it appears that the coating thickness and density do vary on an atomic level depending on the amount of surface moisture present, leaving enough porosity and channels for efficient lithium diffusion.

For long-term cycling, single-layer pouch cells were used instead of coin cells. It is known that materials tend to perform better and more reliably in the former rather than the latter.[27] In manual assembly, main advantages of pouch cells are better alignment of electrodes and gas tightness. Furthermore, pouch cells resemble geometries in industrial applications closer than coin cells do and allow access to larger electrodes for post-mortem analysis.

Figure 3a shows a comparison of the discharge capacity retention in coin and pouch cells, while Figure 3b,c,d gathers the specific discharge capacity, mean discharge voltage, and cell resistance from pouch cell testing. Interestingly, the difference between coated and uncoated NCM851005 CAMs is not as pronounced in pouch cells, since the overall capacity retention is increased. However, it can be observed that the coating improved the mean discharge voltage and reduced the increase in cell resistance over cycling, thereby increasing the cell performance. The Coulombic efficiency is not significantly different, ≈99.90% for both coated and uncoated CAMs.

2.2. Coating of LNO CAM

For coating of the LNO CAM, the process had to be slightly modified to account for the fact that as-synthesized material had very little residual water (<50 ppm), which is necessary for the coating reaction to proceed. On the other hand, the supplied NCM851005 had a water content of ≈600 ppm, as determined by Karl Fischer titration. To address this, an additional processing step was required to introduce moisture and properly coat the material. Specifically, the LNO CAM was dispersed in methanol containing a designated amount of water, then the supernatant liquid was removed and finally the powder was dried in vacuo before being subjected to the coating procedure. Figure S5a,b, Supporting Information, shows the capacity retention and specific discharge capacity of the as-obtained LNO CAMs. As expected, dry LNO (<50 ppm water) coated using the 1.5 equiv.:1.5 equiv. mixture only showed a slightly increased capacity retention versus the uncoated LNO, while wetted LNO (1100 ppm water) revealed a much greater improvement after coating. Notably, the difference between the 2.0 equiv.:1.0 equiv. and 1.5 equiv.:1.5 equiv. coatings was more pronounced than for NCM851005. Unless stated otherwise, coated LNO therefore refers to the 1.5 equiv.:1.5 equiv. coating mixture, which is investigated in more detail in the following paragraphs.

It is known that washing LNO alone can already affect its cycling performance, which can be significantly improved when water as the solvent is avoided.[6,10,28] With the wetting step in methanol and the reaction step in toluene, two washing effects can occur. Figure S5c,d, Supporting Information, shows the capacity retention and specific discharge capacity for LNO that was dispersed in toluene, but not coated and for LNO that was washed in methanol, but not wetted and coated. While the effect of toluene is negligible, the methanol-washed LNO clearly showed increased capacity retention. However, in all cases, the presence of the coating led to the most improved capacity retention.

As in the case of NCM851005 CAM, STEM-EDS of coated LNO confirmed the presence of a coating containing both aluminum and silicon (**Figure 4**a). Figure 4b shows a cavity between two primary particles that, prior to coating, likely contained water due to the capillary effect. After coating, it was filled with a phase containing aluminum and silicon, providing an insight into the reaction of surface moisture with TMA and TEOS.

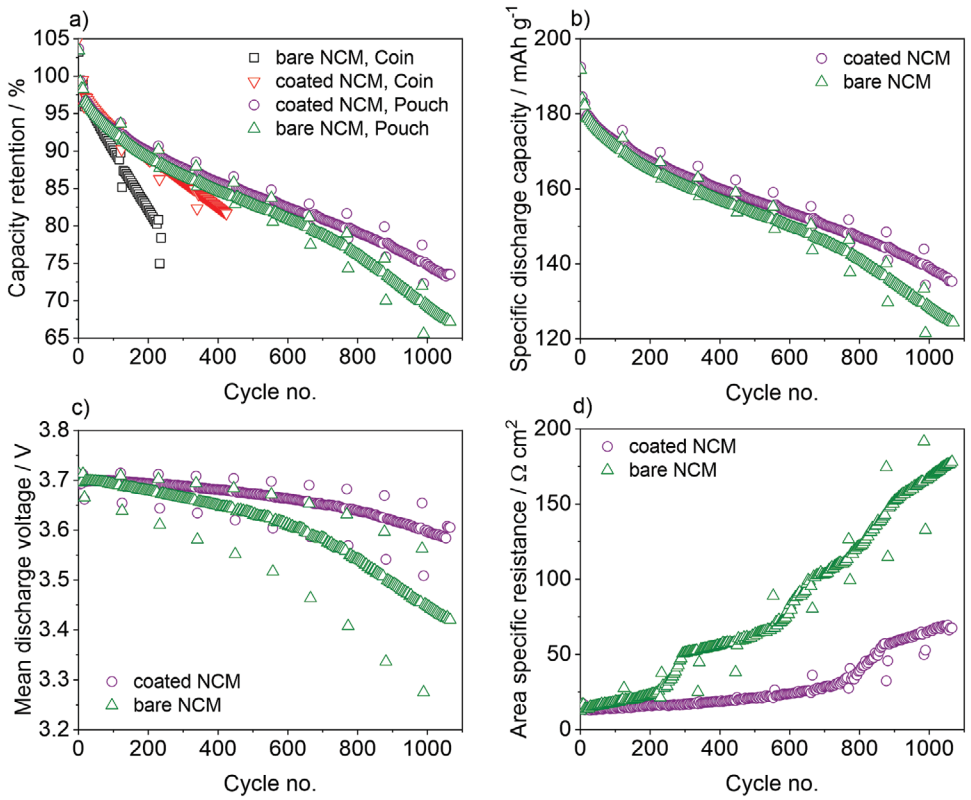

Figure 3. Difference in a) capacity retention, b) specific discharge capacity, c) mean discharge voltage, and d) cell resistance between coated (1.5 equiv.:1.5 equiv.) and uncoated NCM851005 CAMs in pouch full cells. Cells tested at 45 °C, 1.0 C, 3.0–4.2 V.

To quantify the amount of coating, inductively coupled plasma-optical emission spectroscopy (ICP-OES) analysis was carried out. As shown in **Figure 5**, the amounts of silicon and aluminum were similar for both the NCM851005 and wetted LNO CAMs. Furthermore, the surface moisture reaction was proven by clearly increased elemental content in the wetted LNO as opposed to the dry one. The disparity between aluminum and silicon contents, especially after considering the silicon already present in the uncoated CAM, can be explained by the higher reactivity of TMA compared to TEOS.

Recently, a long-term pouch cell study has been reported for LNO.[26] In a similar fashion, yet with differences in cell assembly and under different cycling conditions, both the 1.5 equiv:1.5 equiv. and 2.0 equiv.:1.0 equiv. coatings were compared to bare LNO, providing a second data set of LNO long-term performance. As depicted in **Figure 6**a, the capacity retention achieved with the two different coating mixtures is very similar in pouch cells and notably improved compared to that of bare LNO. Cells using the bare LNO on average fell below 80% capacity retention after 69 cycles, while cells with the coated LNO on average lasted 205 cycles, an improvement by a factor of three. Figure 6b–d shows that other relevant cell characteristics are also improved, as well as the fact that there is only a minor advantage of the equimolar coating reagent mixture over the 2:1 ratio in terms of cell resistance and mean discharge voltage. It is noteworthy that the specific capacity in the first cycle was decreased by only 5.2 mAh g_{CAM}^{-1} (214.5 vs 219.7 mAh g_{CAM}^{-1}) compared to uncoated LNO. The average Coulombic efficiency was above 99.91%.

2.3. Post-Mortem Analysis

After completion of the long-term cycling (1100 cycles), the LNO pouch cells were disassembled and the electrodes harvested. **Figure 7**a–c shows results from STEM imaging and electron energy-loss spectroscopy (EELS) elemental mapping of surface regions of coated and uncoated secondary particles. It can be seen that a ≈10 nm coating was still present after cycling. Additionally, a fluorine-containing layer was apparent both on coated and uncoated particles, with the layer being more diffuse around uncoated particles.

Detailed study of the Ni—$L_{2,3}$ edge reveals its chemical shift of ≈1 eV to lower energy near the LNO particle surface (Figure S6, Supporting Information). Figure 7d,e shows the chemical shift mapped using the multiple linear least squares (MLLS) fitting routine in Gatan Digital Micrograph. The maps indicate a surface layer thickness of ≈8 nm in coated and 20–30 nm in uncoated LNO. The Ni—$L_{2,3}$ edge shift provides evidence that the Ni cations are in different valence states near the particle surface compared to the bulk. Note that the Ni reduction observed near the surface is indicative of the formation of a rock salt-type $Li_xNi_{1-x}O$ layer, as is often reported in the literature.[29–33] The presence of the rock salt-type structure was also confirmed by high-resolution STEM (HR-STEM), see

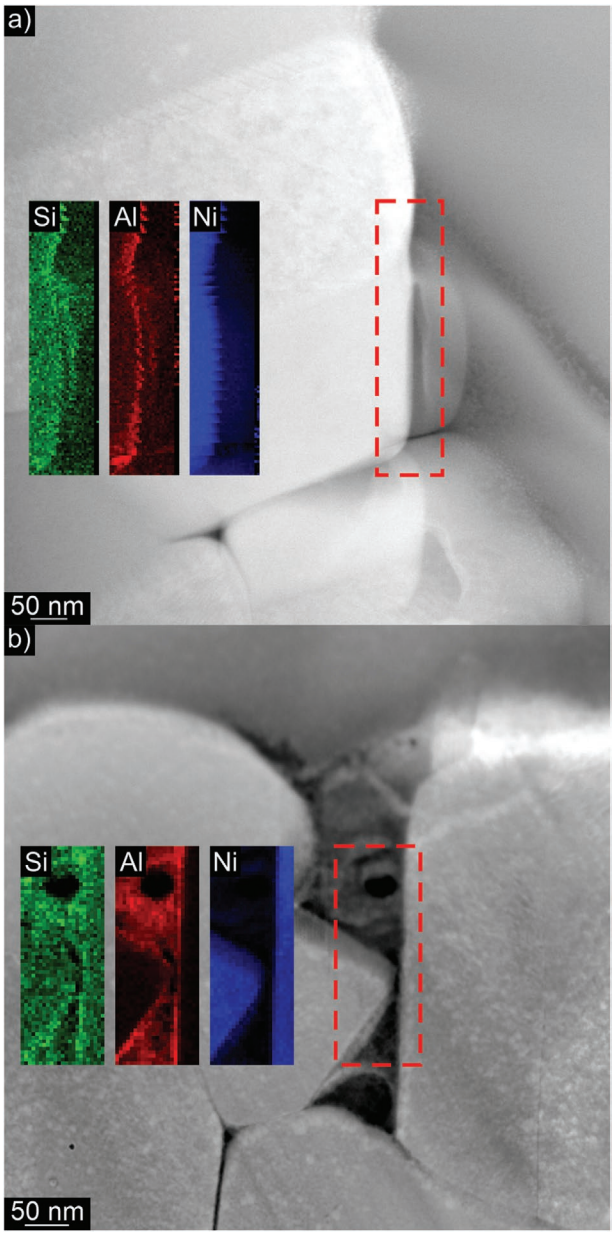

Figure 4. STEM-EDS analysis of a) the outer surface of a coated (1.5 equiv.:1.5 equiv.) LNO particle and b) a cavity between two primary particles.

Figure 7f,g. In the bulk, a characteristic pattern of the layered structure with bright rows of Ni cations spaced by 4.84 Å [(003) crystallographic plane] is observed. The pattern changes at the surface, where the contrast becomes homogeneous. These findings are corroborated by the corresponding fast Fourier transforms (FFTs). The TEM investigation of the interface between two primary particles in coated and uncoated LNO CAMs is detailed in Figure S7, Supporting Information, showing smooth edges and a clear gap for coated LNO, but rough edges and a gap diffusely filled with oxygen, fluorine, and nickel for uncoated LNO. The match in location of fluorine and nickel, also in Figure 7, suggests the presence of NiF_2[34] as a degradation product from acid leaching, which is further evident from

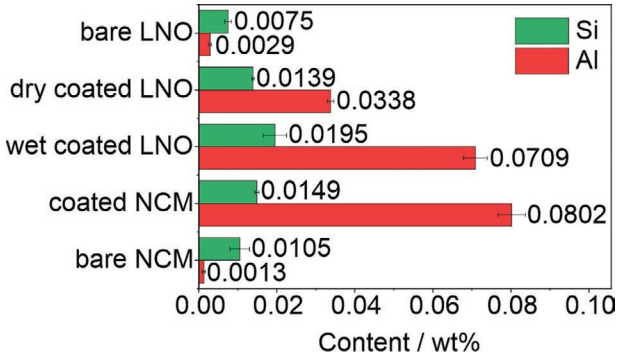

Figure 5. ICP-OES results for uncoated and coated (1.5 equiv.:1.5 equiv.) NCM851005 and LNO CAMs.

TEM results for cycled NCM851005 CAMs (see Figures S8 and S9, Supporting Information). For uncoated NCM851005, surface corrosion can be observed. This is caused by the dissolution of transition-metal ions promoted by hydrogen fluoride.[35] Together with protons, lattice oxygen at the LNO surface forms water, receiving electrons from Jahn–Teller active Ni^{3+} in the process. The resulting Ni^{4+} readily oxidizes electrolyte molecules and thereby is reduced to soluble Ni^{2+}.[36] As the formed water again reacts with $LiPF_6$, new hydrogen fluoride is formed, allowing the leaching to continue.

The Ni content of the harvested anodes (1100 cycles) was analyzed via ICP-OES to confirm whether dissolution and migration across the cell occurred.[37,38] Ni contents of (0.0294 ± 0.0004) wt% in a cycled anode paired with cathodes of coated LNO and (0.0429 ± 0.0006) wt% in an anode paired with cathodes of uncoated LNO suggest that the protective surface layer also mitigates metal leaching, as has been reported before.[39]

Using XPS, the surface of the coated cathodes was investigated in more detail. As shown in **Figure 8**, the binding energy of the Al 2p peak was increased by 0.9 eV for (cycled) coated LNO CAM when compared to fresh cathodes. Figure S10, Supporting Information, shows a similar finding for NCM851005. This increase in binding energy is indicative of a fluorine-scavenging effect of the coating, leading to a change from oxide to oxyfluoride environment for the aluminum ions, as also suggested by the fluorine-containing layer observed by TEM (Figure 7) and described in the literature.[34,40,41] Figure S11, Supporting Information, shows the Al 2p XP spectra of coated and uncoated CAM powder samples. Silicon (Si 2p) was probed via XPS too, but because of residual silicon in the particles and the low amount of coating, no clear effect could be observed.

2.4. Gassing Analysis

Although some in situ data are available on the gas evolution of Ni-rich (>80% Ni content) NCM CAMs or even LNO, open questions remain because of the difficult comparability between experimental setups.[28,42–45] Moreover, no studies have been published yet on the influence of coatings on the gas evolution of layered oxides in LIBs.[5,45] Here, our DEMS analysis focuses on carbon dioxide (CO_2) evolution, the most prevalent gas released by far.[42,46] CO_2 can be produced by decomposition of surface carbonate impurities, electrochemical oxidation of

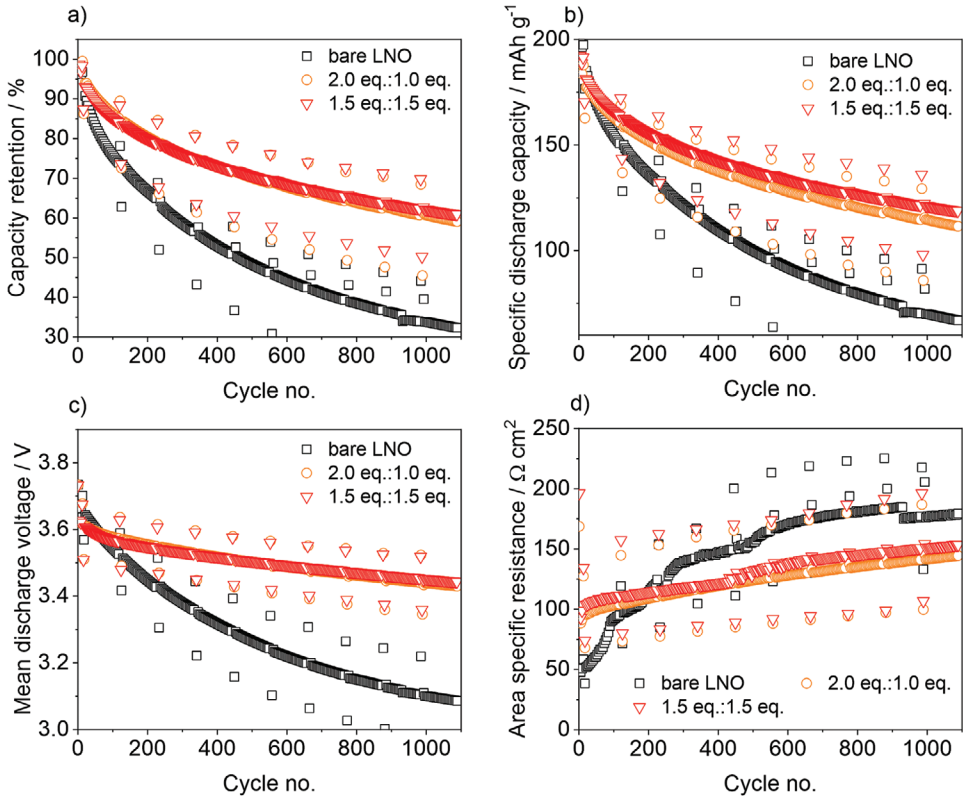

Figure 6. Performance of LNO pouch full cells. Difference in a) capacity retention, b) specific discharge capacity, c) mean discharge voltage, and d) cell resistance between coated and uncoated LNO CAMs. Cells tested at 25 °C, 1.0 C, 3.0–4.2 V.

organic carbonate electrolyte, and chemical oxidation involving oxygen released from the lattice during transformation to the rock salt-type phase.[42,46,48] Recently, it was shown that decomposition of surface carbonates contributes especially to the CO_2 evolution in the initial cycle,[46] while in later cycles, CO_2 is formed by reaction of the reactive singlet oxygen ($^1O_2$) released from the CAM lattice with the electrolyte.[47] However, CO_2 evolution also strongly depends on the cut-off voltage and achieved state of charge (i.e., degree of delithiation).[42,44,46–48] Regardless of the CO_2 origin, greatly reduced gassing is expected to have a beneficial effect on the electrochemical performance and, from a practical point of view, on safety.

NCM851005 and LNO, each coated using the 1.5 equiv.:1.5 equiv. mixture of TMA and TEOS, were investigated via DEMS and compared to the respective uncoated CAMs. For NCM851005, **Figure 9** shows a summary of specific charge capacities and total CO_2 amounts for the first two cycles. As coated and uncoated NCM851005 showed similar capacities, hence, nearly equivalent states of charge, the amounts of evolved CO_2 can be directly compared. Uncoated NCM851005 released 62.4 µmol g_{CAM}^{-1} combined, while coated CAM only released 10.1 µmol g_{CAM}^{-1}. The coating therefore lowered the total gas evolution by a factor of more than six. The difference between the first and second cycles can mostly be explained by the decomposition of surface carbonates in the initial cycle, as previously mentioned.[46]

For LNO, one has to consider the initially lower specific charge capacity of coated versus uncoated CAM that is likely caused by the higher resistance of the coated LNO, as shown in Figure 6. Consequently, reductions in gas evolution cannot be univocally attributed to the coating, but also to the effect of a lower state of charge. Further detailed analysis and discussion of the dependence of gassing on the state of charge for coated and uncoated CAMs is currently under investigation, but goes beyond the scope of this paper.

2.5. Discussion

From the observations made so far, we found multiple effects of the coating that can explain the reported increase in performance. First, the reduced thickness of the rock salt-type surface layer, as shown in Figure 7. Second, the reduced gas evolution, as shown in Figure 9. Third, the scavenging of HF, as indicated by the dense fluorine-containing layer in Figure 7 and the change in chemical environment of aluminum in Figure 8. Acid scavenging in turn prevents transition-metal leaching. It should be mentioned that the formation of AlF_3 from alumina coatings has been reported not only as a result of HF scavenging, but also because of the reaction with $LiPF_6$ in the electrolyte, forming $LiPO_2F_2$ as a beneficial electrolyte additive.[14] So far, presumably due to the very small amount of coating elements present, the role of Si has not been determined and remains to be discussed. From ICP spectroscopy, an Al/Si ratio of 5.9 for LNO and 18.6 for NCM851005 is found, which can be explained by the higher reactivity of TMA compared to TEOS.

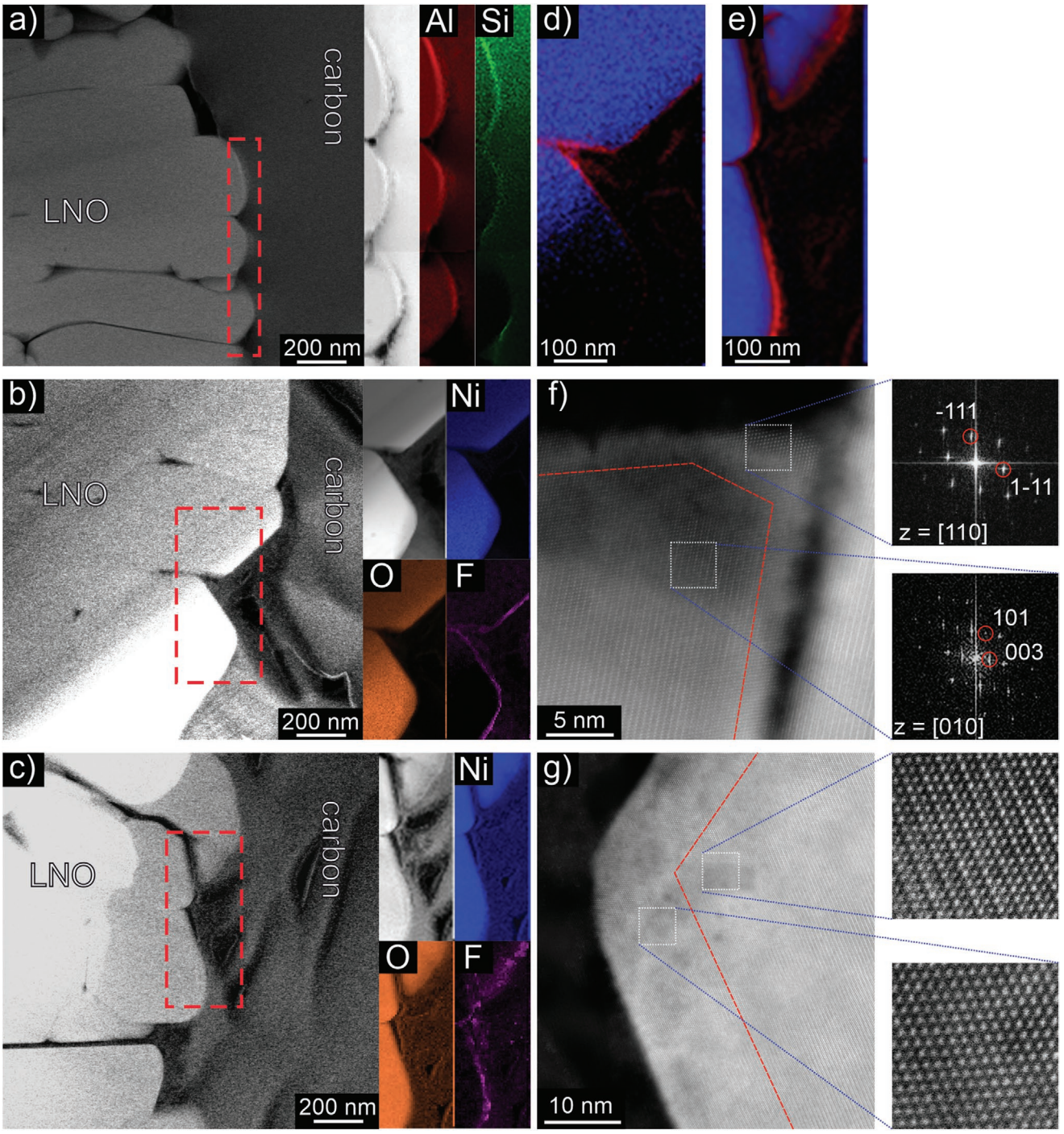

Figure 7. STEM imaging and EELS mapping of a,b) coated (1.5 equiv.:1.5 equiv.) and c) uncoated LNO after long-term cycling and mapping of Ni valence state (red: +2, blue: +3) in d) coated and e) uncoated CAMs. HR-STEM images confirm the presence of a rock salt-type layer of different thicknesses for f) coated and g) uncoated LNO.

As both reagents are in contact with the CAM at the same time and compete for surface moisture or hydroxides as reaction partners, it can be assumed that the local distribution of coating elements varies to some degree such that not a single composition is achieved, but multiple possible compositions of the type $Li_xAl_ySi_zO$ (plus alumina and silica) are present at the same time at different spots. A similar observation of $Li_x[Al_ySi_zO_4]$ has been made for manganese-rich cathodes, where an optimal combination of Al_2O_3 and SiO_2 in the ratio of 2:1 was reported, yet at a much higher coating mass fraction.[49]

We suggest that additional to the positive effect of alumina, the high affinity of silicon and fluorine leads to the formation of fluorinated species, of which mostly SiF_4 and Li_2SiF_6 have been discussed in the literature,[20,22,50,51] while a variety

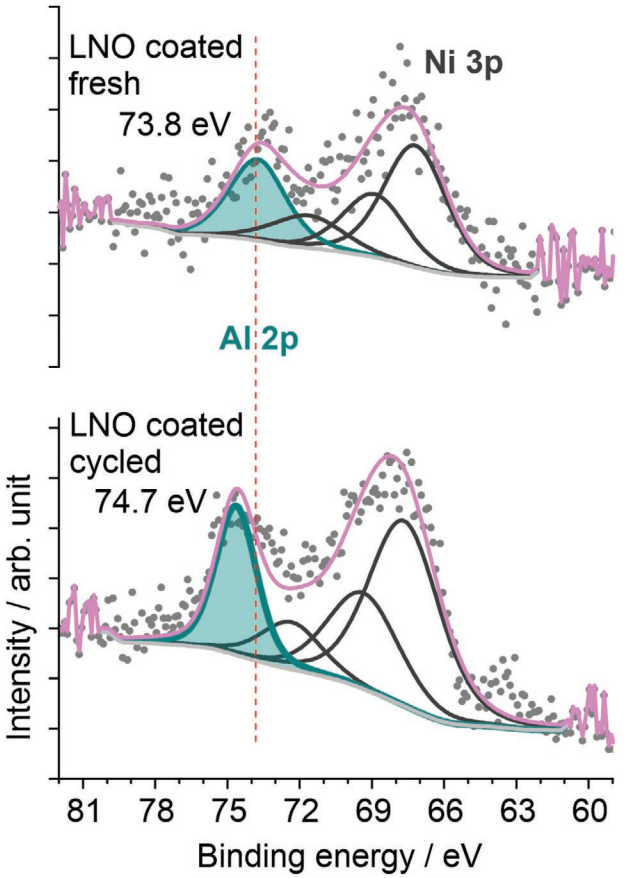

Figure 8. Increase in Al 2p peak-binding energy after cycling of the LNO CAM suggesting a change in chemical environment of the Al ions from oxide to oxyfluoride or fluoride.

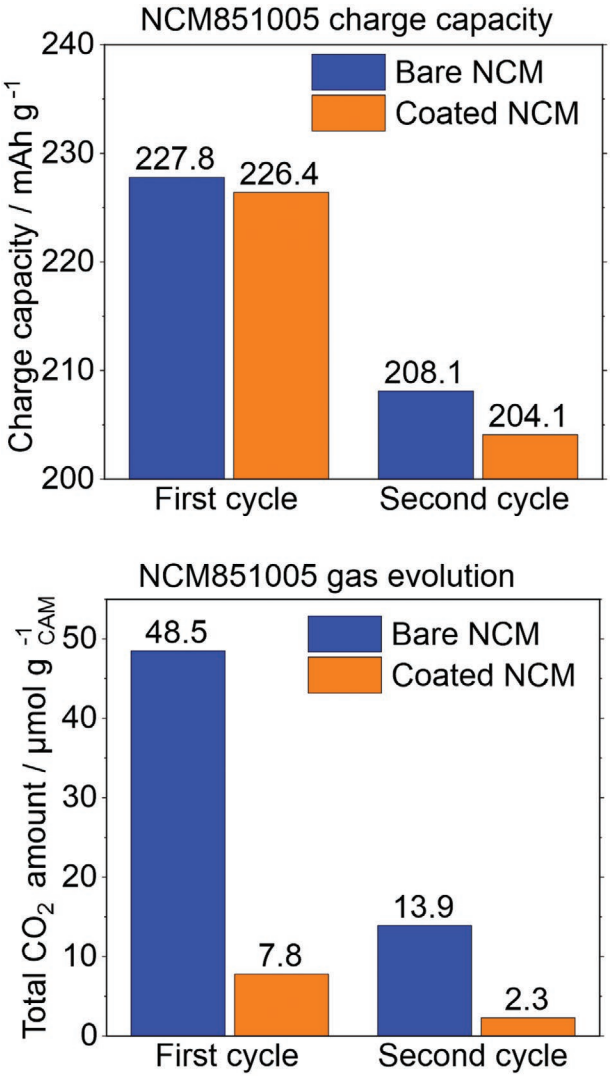

Figure 9. DEMS measurements on NCM851005 CAMs. Cells tested at 25 °C, 0.1 C, 3.0–4.3 V versus Li^+/Li.

of oxyfluorides are also known.[52] These species might either retain fluorine permanently as a scavenger or react with alumina, as applied in aluminum refining,[53] forming an oxyfluoride environment (see also section on XPS above). Because the coating still contains silicon after 1100 cycles, mobile (gaseous) species, such as SiF_4, either reacted before leaving the layer or their formation was disfavored versus less mobile species. In DEMS, the formation (or non-formation) of SiF_4 can only be monitored by following the $m/z = 85$ signal of SiF_3^+, where also POF_2^+, the main fragment of POF_3, a known gassing product,[54,55] is detected.

Furthermore, the formation of silicates, such as Li_2SiO_3[23] and Li_4SiO_4,[21] has been reported to support lithium diffusion and protection of the CAM. Beyond the abovementioned acid scavenging at the cathode side,[19] silica is also used in separators[50] and composite electrolytes[56,57] to increase cell performance, providing further support to its beneficial role within the cell. Additionally, silica and aluminosilicates have been shown to quench $^1O_2$.[58,59] As the oxygen released from the layered CAM lattice is apparently $^1O_2$,[48,60] we hypothesize a conversion of highly reactive singlet oxygen to less reactive triplet oxygen as an additional stabilization mechanism.

To address whether the beneficial effect of the TMA:TEOS combination is specific to the respective elements, experiments were carried out in a similar fashion with trimethylgallium and trimethylbismuth and their combinations with TMA. However, they did not lead to satisfactory results. While the exact reason is unclear at present, often observed rollover failure points at issues of coating stability and metal deposition on the anode side.

In summary, we propose that alumina and silica coatings on their own act via different protective mechanisms and a combination of both materials therefore shows a synergistic effect by merging these mechanisms, most likely within an aluminosilicate-type structure.

3. Conclusion

In this work, a liquid-phase binary coating approach was applied to two promising next-generation Ni-rich CAMs, namely, NCM851005 and LNO. For NCM851005, multiple experiments were performed to examine the performance of different coating compositions and amounts. It was found

that the optimal coating is obtained from a reaction mixture of 150 µmol each of TMA and TEOS per 1 g of NCM851005, whereas higher reagent amounts reduce the initial specific capacity and lower reagent amounts, as well as different ratios, lead to accelerated capacity fading. ICP-OES clarified that the same amounts of precursors do not necessarily lead to a coating with equimolar amounts of silicon and aluminum.

The results of the study on NCM851005 were transferred to LNO via the inclusion of an additional wetting step. This procedure enabled achieving a successful coating, as proven not only by cell performance, but also by SEM, TEM, and ICP-OES. In pouch cells, uncoated LNO lasted an average of 69 cycles before reaching 80% of its original capacity, while cells with LNO coated by the aforementioned optimal mixture lasted an average of 205 cycles, which is a drastic improvement by a factor of three. After long-term cycling for almost 1100 cycles, electrodes (NCM851005, LNO, graphite) were harvested and investigated using TEM, ICP-OES, and XPS. It was found that in coated LNO, a much thinner rock salt-type layer had formed on the surfaces compared to uncoated LNO. While the coating appeared to be intact after cycling, it now also contained fluoride, while in uncoated LNO, the fluoride layer seemed more diffuse. This result suggests a fluorine-scavenging effect of the coating, as supported by the observation of increased Al 2p peak-binding energy via XPS. Using ICP-OES, the Ni content of anodes paired with coated LNO was found to be lower than that of anodes paired with uncoated LNO, indicating that the coating also reduces metal leaching.

The outgassing of NCM851005 during battery operation was investigated by DEMS. The coating drastically reduced the gas evolution, which at least to some extent, is responsible for improved electrochemical performance. As carbon dioxide (after the 1st cycle) mostly stems from the reaction of released lattice oxygen with the electrolyte components, the detrimental high-voltage phase transformation appears to be reduced, as also confirmed by post-mortem TEM.

In conclusion, we proved that the synergetic effect of Al and Si yields an oxide coating suitable to stabilize CAMs with a Ni content up to 100%. The coating protects the materials by scavenging HF and reducing the amount of transition-metal dissolution, as well as by reducing the outgassing at high states of charge. Both effects ultimately lead to lower impedance increase and better capacity retention in pouch full cells. In future studies, more detailed investigations into the role of Si and the scavenging mechanism are envisioned. The use of a non-hydrolyzing electrolyte salt, such as $Li[(C_2F_5)_3PF_3]$,[61] instead of $LiPF_6$ and the resulting reduced formation of HF may provide an insight into what extent HF scavenging is explaining the effect of the coating and to what extent other protective mechanisms are involved. Because other organometallic reagents can be used in the experimental procedure, different coating compositions and elemental combinations open up space for future studies.

4. Experimental Section

Unless stated otherwise, all preparative steps were performed in a glovebox (MB200B, MBraun) under an argon atmosphere with oxygen and water levels below 0.1 ppm. NCM851005 was supplied by BASF SE and used as received. LNO was prepared as reported in the literature.[62]

LNO Synthesis: $LiNiO_2$ was prepared from $Ni(OH)_2$ and Li(OH) H_2O (BASF SE). After thoroughly mixing $Ni(OH)_2$ (12.981 g, 0.140 mol, 1.00 equiv.) and LiOH H_2O (5.933 g, 0.141 mol, 1.01 equiv.), the resulting mixture was heated in oxygen flow (5 L h^{-1}, ≈0.65 reactor volume exchanges per h) in a box furnace (VMK-80-S, Linn High Term) at 700 °C for 6 h, with heating and cooling rates set to 3 °C min^{-1}. The calcination product was rapidly transferred into the glovebox and sieved with a 45 µm metal sieve, yielding 13.272 g LNO. LNO purity was confirmed by X-ray diffraction (XRD) and multiple batches were blended to ensure uniform properties.

To obtain wetted LNO, an amount of 3.5 g LNO was dispersed in a solution of 15 µL deionized water in 5 mL dry methanol, and the dispersion was shaken for 5 min. The supernatant liquid phase was removed with a syringe and the LNO dried at room temperature and 1×10^{-3} mbar on a Schlenk line for 2 h. Wetting was confirmed by Karl Fischer titration, indicating a water content in the range between 1100 and 1200 ppm, in contrast to a water content below the detection limit for dry (as-synthesized) LNO.

Coating Reaction: An oven-dried Schlenk flask containing a magnetic stirring bar was transferred to the glovebox and 7 mL dry toluene (Sigma–Aldrich) added into the flask. The reagents were then added dropwise. For TMA, a 2 M solution in toluene (Sigma–Aldrich) was used. TEOS (Merck KGaA) was used as received. For readability and easy comparison, the reagent amount was given in equivalents of a base amount of 100 µmol reagent per 1 g of CAM. After adding the reagents, the solution was stirred for 1 h and then 2.5 g CAM was added. After 2 h, the flask was transferred to a Schlenk line with a cold trap between line and flask to remove solvent and excess reagents in vacuo. After no liquid phase was visible anymore, the flask was directly attached to the Schlenk line and the CAM dried at room temperature and 1×10^{-3} mbar overnight. The obtained material was heated at 300 °C in a tube furnace (P330, Nabertherm) in oxygen flow (1 L h^{-1}, ≈1.5 reactor volume exchanges per h) for 1 h. The heating and cooling rates were set to 2.3 °C min^{-1}. Afterward, the product was rapidly transferred back into the glovebox.

Cathode Preparation: The cathode slurries necessary for electrode fabrication were prepared by first mixing a 7.5 wt% binder solution of polyvinylidene difluoride (PVDF, Solef 5130, Solvay) in *N*-methyl-2-pyrrolidone (NMP, ≥99.5%, Merck KGaA) with conductive carbon black (Super C65, TIMCAL Ltd.) and NMP in a planetary centrifugal mixer (ARE-250, Thinky) for 3 min at 2000 rpm, followed by 3 min at 400 rpm. After the first mixing, the CAM was added to the slurry. For LNO, a sealable screw-cap mixing cup was used and the CAM added inside the glovebox. For NCM851005, an open mixing cup was used. The mixture was then stirred again for 3 min at 2000 rpm and 3 min at 400 rpm, yielding a homogenous deep black slurry. Using a motorized film applicator (Erichsen Coatmaster 510), the slurry was immediately coated on 0.03 mm thick aluminum foil with a blade film applicator having a slit height of either 120 µm for NCM851005 or 140 µm for LNO to achieve areal loadings of ≈10 mg_{CAM} cm^{-2}. The resulting cathode tapes were dried at 120 °C in vacuo overnight and afterward calendared at 15 N mm^{-1} (Sumet Messtechnik). Coin-cell cathodes were punched out using an arc punch of 14 mm. Pouch cell cathodes were punched out using a 20×40 mm^2 die. For DEMS-cell cathodes, a circular die with an inner diameter of 4 mm and an outer diameter of 30 mm was used.

Cell Preparation: CR2032 steel coin cells (Hohsen Corp.) were assembled inside the glove box with a vacuum pen by placing cathode, gasket ring, and separator in the case, then soaking with electrolyte and adding the anode, spacer disk, and spring before closing the cell by slightly pressing the cap into the gasket ring. The cells were sealed by crimping (MSK-160D, MTI Corp.). A 17 mm polyethylene fiber separator (Freudenberg), 50 µL LP472 electrolyte (1.0 M $LiPF_6$ in 3:7 ethylene carbonate [EC]:diethyl carbonate [DEC] by weight with 2% vinylene carbonate additive), and a 15 mm diameter graphite anode (≈8 mg cm^{-2}) were used. Single-layer pouch cells were assembled in a dry room (dew point < −55 °C) using a 50×30 mm^2 microporous

polypropylene separator (Celgard 2500), 500 µL LP472 electrolyte, and a 42 × 22 mm² graphite anode. The n/p ratio[63] was controlled by choosing adequate electrode loadings based on the initial specific capacity in half-cells (LNO : 250 mAh g^{-1}, NCM851005 : 235 mAh g^{-1}, graphite: 330 mAh g^{-1}). With a graphite loading of 64 mg per pouch cell anode, n/p ratios of 1.16 for LNO (73 mg CAM per pouch cell cathode) and 1.32 for NCM851005 (68 mg CAM per pouch cell cathode) were achieved. The lower n/p ratio for LNO was chosen to partially accommodate the increased initial loss of cathode capacity.[64]

Electrochemical Testing: In general, for every experiment, at least three cells were successfully cycled and results are shown as the average of these cells. They were cycled in a battery testing system (Series 4000, MACCOR) at 45 °C to stress the CAM in order to observe performance differences earlier, or in case of LNO pouch cells, at 25 °C to ensure comparability with most other LNO cycling studies.[26] The first two cycles involved galvanostatic charging to 4.2 V (full cells) or 4.3 V (half-cells) at a rate of 0.1 C, with 1 C = 195 mA g_{CAM}^{-1} for NCM851005 and 225 mA g_{CAM}^{-1} for LNO. After reaching the cut-off voltage, the charge was continued for either 1 h or until the current dropped below 0.02 C depending on which condition was met first. After 5 min of rest, the cells were discharged to 2.8 V at 0.1 C rate and then rested for 5 min. After these initial cycles, the charge rate was set to 0.5 C. The discharge rate was 1 C for the first ten cycles, then a rate test with two cycles each at 0.5, 1, 2, and 3 C followed. For long-term cycling, the rate test was repeated after 100 cycles at 1 C each.

For NCM851005, coin-cell testing was ended automatically after 425 cycles or when the discharge capacity fell below 80% of the specific capacity delivered in the 3rd cycle. For LNO and all pouch cells, the test was carried out beyond this and ended manually. Capacity retention was reported as the share of capacity in a given cycle compared to the 3rd cycle capacity of the cell in question. The cell resistance was calculated once per cycle from the voltage difference between the last data point of rest after constant-voltage charge and the interpolated voltage after 1 s of discharge at the given discharge current. Thus, the reported resistance is that of a cell after completed charge.

Gas Analysis: The gas evolution was studied by differential electrochemical mass spectrometry (DEMS). A specialized cell made from a 30 mm diameter cathode with a 4 mm hole in the center allowed for gas flow, a 40 mm diameter GF/D glass microfiber separator (Whatman), a 32 mm diameter Li-metal anode, and 800 mL LP57 electrolyte (1.0 M $LiPF_6$ in 3:7 EC:ethyl methyl carbonate [EMC]) was cycled in the voltage range between 2.8 V and 4.3 V versus Li^+/Li at 0.1 C rate. During cycling, a constant stream of He carrier gas (purity 6.0, 2.5 mL min^{-1}) was passed through the cell. The extracted gas mixture was analyzed using a mass spectrometer (Omni Star GSD 320, Pfeiffer Vacuum GmbH). Further details can be found in the literature.[65,66]

Karl Fischer Titration: Coulometric Karl Fischer titration was carried out using an 851 Titrando setup (Metrohm). About 500 mg sample was heated to 250 °C in an oven module (860 KF Thermoprep, Metrohm) under a stream of dry air toward the measurement cell. The detection limit of the setup is ≈10 µg, with a quantification limit of ≈50 µg for water.

Electron Microscopy: Scanning electron microscopy (SEM) was carried out with a Leo 1530 SEM (Zeiss) equipped with a Schottky-type field-emission gun at accelerating voltages of 10 or 20 kV with an in-lens secondary electron detector. Energy dispersive X-ray spectroscopy (EDS) was carried out at 20 kV using an Oxford X-Max^N (Oxford Instruments) detector.

Transmission electron microscopy (TEM) of powder samples was performed using a Titan 80–300 image-corrected microscope (FEI) equipped with an EDAX EDS detector. The study of tapes was performed on a Themis Z (Thermo Fisher Scientific) double-corrected transmission electron microscope operated at 300 kV. Samples for TEM investigation were prepared by lift-out technique using a gallium focused-ion beam (FIB) on a STRATA dual-beam system. The samples were milled at 30 kV followed by final polishing at 2 kV to reduce surface-layer damage. Scanning TEM (STEM) images were collected using a high-angle annular dark-field (HAADF) detector. EELS data were acquired with an energy resolution of ≈1 eV, estimated by the full width at half maximum of the zero-loss peak (ZLP) by a Gatan image filter with continuum camera (Gatan Inc.). The spectra were collected in dual EELS mode, allowing to lock the ZLP and use it as a reference for accurate determination of the edge position of each element.

ICP-OES: For ICP-OES, the samples were dissolved in acid in a graphite furnace and unless stated otherwise, mass fractions of specified elements were measured three times per sample.

XPS: X-ray photoelectron spectroscopy (XPS) measurements were performed using a K-Alpha instrument (Thermo Fisher Scientific) applying a micro-focused, monochromatic Al-K_α X-ray source with a 400 µm spot size. The samples were transported under inert atmosphere for XPS analysis. Data acquisition and processing using the Thermo Avantage software is described in ref. [67]. The K-Alpha charge-compensation system was employed during the analysis using electrons of 8 eV energy and low-energy argon ions to prevent localized charge buildup. The spectra were fitted with one or more Voigt profiles. All spectra are referenced to the C 1s peak of either hydrocarbon at 285.0 eV or graphitic carbon at 284.4 eV controlled through well-known photoelectron peaks of Cu, Ag, and Au. For intense peaks and/or peaks clearly evidenced by the peak shape, the binding energy uncertainty was ±0.1 eV. In the case of weak peaks and no direct justification by the peak shape, the uncertainty was set to ±0.2 eV. The analyzer transmission function, Scofield's sensitivity factors,[68] and effective attenuation lengths (EALs) for photoelectrons were applied for quantification. The EALs were calculated using the standard TPP-2M formalism.[69]

Supporting Information

Supporting Information is available from the Wiley Online Library or from the author.

Acknowledgements

This study was supported by BASF SE. The authors thank Dr. Thomas Bergfeldt (KIT, IAM-AWP) for ICP-OES analysis. Sören L. Dreyer wishes to thank the Studienstiftung des Deutschen Volkes for support.

Open access funding enabled and organized by Projekt DEAL.

Conflict of Interest

The authors declare no conflict of interest.

Data Availability Statement

The data that support the findings of this study are available from the corresponding author upon reasonable request.

Keywords

aluminosilicate, layered Ni-rich oxide cathodes, lithium nickel oxide, lithium-ion batteries, surface coating

Received: June 29, 2021
Revised: September 26, 2021
Published online:

[1] W. Li, E. M. Erickson, A. Manthiram, *Nat. Energy* **2020**, *5*, 26.
[2] S.-T. Myung, F. Maglia, K.-J. Park, C. S. Yoon, P. Lamp, S.-J. Kim, Y.-K. Sun, *ACS Energy Lett.* **2017**, *2*, 196.

[3] L. de Biasi, A. O. Kondrakov, H. Geßwein, T. Brezesinski, P. Hartmann, J. Janek, *J. Phys. Chem. C* **2017**, *121*, 26163.
[4] H.-J. Noh, S. Youn, C. S. Yoon, Y.-K. Sun, *J. Power Sources* **2013**, *233*, 121.
[5] F. Schipper, E. M. Erickson, C. Erk, J.-Y. Shin, F. F. Chesneau, D. Aurbach, *J. Electrochem. Soc.* **2017**, *164*, A6220.
[6] M. Bianchini, M. Roca-Ayats, P. Hartmann, T. Brezesinski, J. Janek, *Angew. Chem., Int. Ed.* **2019**, *58*, 10434.
[7] F. Schipper, P. K. Nayak, E. M. Erickson, S. F. Amalraj, O. Srur-Lavi, T. R. Penki, M. Talianker, J. Grinblat, H. Sclar, O. Breuer, C. M. Julien, N. Munichandraiah, D. Kovacheva, M. Dixit, D. T. Major, B. Markovsky, D. Aurbach, *Inorganics* **2017**, *5*, 32.
[8] H. H. Sun, H.-H. Ryu, U.-H. Kim, J. A. Weeks, A. Heller, Y.-K. Sun, C. B. Mullins, *ACS Energy Lett.* **2020**, *5*, 1136.
[9] H. Zhu, H. Yu, H. Jiang, Y. Hu, H. Jiang, C. Li, *Chem. Eng. Sci.* **2020**, *217*, 115518.
[10] D. Weber, Đ. Tripković, K. Kretschmer, M. Bianchini, T. Brezesinski, *Eur. J. Inorg. Chem.* **2020**, *2020*, 3117.
[11] H. Yu, Y. Li, Y. Hu, H. Jiang, C. Li, *Ind. Eng. Chem. Res.* **2019**, *58*, 4108.
[12] H. Yu, S. Wang, Y. Hu, G. He, L. Q. Bao, I. P. Parkin, H. Jiang, *Green Energy Environ.* **2020**, https://doi.org/10.1016/j.gee.2020.09.011.
[13] S.-T. Myung, K. Izumi, S. Komaba, Y.-K. Sun, H. Yashiro, N. Kumagai, *Chem. Mater.* **2005**, *17*, 3695.
[14] D. S. Hall, R. Gauthier, A. Eldesoky, V. S. Murray, J. R. Dahn, *ACS Appl. Mater. Interfaces* **2019**, *11*, 14095.
[15] D. Mohanty, K. Dahlberg, D. M. King, L. A. David, A. S. Sefat, D. L. Wood, C. Daniel, S. Dhar, V. Mahajan, M. Lee, F. Albano, *Sci. Rep.* **2016**, *6*, 26532.
[16] M. J. Herzog, N. Gauquelin, D. Esken, J. Verbeeck, J. Janek, *Energy Technol.* **2021**, *9*, 2100028.
[17] L. A. Riley, S. Van Atta, A. S. Cavanagh, Y. Yan, S. M. George, P. Liu, A. C. Dillon, S.-H. Lee, *J. Power Sources* **2011**, *196*, 3317.
[18] S. Neudeck, F. Strauss, G. Garcia, H. Wolf, J. Janek, P. Hartmann, T. Brezesinski, *Chem. Commun.* **2019**, *55*, 2174.
[19] W. Cho, S.-M. Kim, J. H. Song, T. Yim, S.-G. Woo, K.-W. Lee, J.-S. Kim, Y.-J. Kim, *J. Power Sources* **2015**, *282*, 45.
[20] L. Liang, G. Hu, F. Jiang, Y. Cao, *J. Alloys Compd.* **2016**, *657*, 570.
[21] J. Zheng, Z. Yang, Z. He, H. Tong, W. Yu, J. Zhang, *Nano Energy* **2018**, *53*, 613.
[22] Y. Chen, S. Tang, S. Deng, T. Lei, Y. Li, W. Li, G. Cao, J. Zhu, J. Zhang, *J. Power Sources* **2019**, *431*, 8.
[23] X. Deng, K. Wu, R. Dang, N. Li, H. Zhang, J. Jiao, Y. Lee, Z. Hu, X. Xiao, *J. Electrochem. Soc.* **2021**, *168*, 050539.
[24] D. Zuo, C. Wang, G. Tian, K. Shu, X. Liu, *J. Electrochem. Sci. Eng.* **2019**, *9*, 85.
[25] Y.-C. Perng, J. Cho, S. Y. Sun, D. Membreno, N. Cirigliano, B. Dunn, J. P. Chang, *J. Mater. Chem. A* **2014**, *2*, 9566.
[26] A. Mesnier, A. Manthiram, *ACS Appl. Mater. Interfaces* **2020**, *12*, 52826.
[27] V. Murray, D. S. Hall, J. R. Dahn, *J. Electrochem. Soc.* **2019**, *166*, A329.
[28] D. Pritzl, T. Teufl, A. T. S. Freiberg, B. Strehle, J. Sicklinger, H. Sommer, P. Hartmann, H. A. Gasteiger, *J. Electrochem. Soc.* **2019**, *166*, A4056.
[29] F. Lin, I. M. Markus, D. Nordlund, T.-C. Weng, M. D. Asta, H. L. Xin, M. M. Doeff, *Nat. Commun.* **2014**, *5*, 3529.
[30] C. S. Yoon, D.-W. Jun, S.-T. Myung, Y.-K. Sun, *ACS Energy Lett.* **2017**, *2*, 1150.
[31] H. Liu, M. Bugnet, M. Z. Tessaro, K. J. Harris, M. J. R. Dunham, M. Jiang, G. R. Goward, G. A. Botton, *Phys. Chem. Chem. Phys.* **2016**, *18*, 29064.
[32] P. Yan, J. Zheng, J.-G. Zhang, C. Wang, *Nano Lett.* **2017**, *17*, 3946.
[33] P. Mukherjee, P. Lu, N. Faenza, N. Pereira, G. Amatucci, G. Ceder, F. Cosandey, *ACS Appl. Mater. Interfaces* **2021**, *13*, 17478.
[34] H. Hemmelmann, J. K. Dinter, M. T. Elm, *Adv. Mater. Interfaces* **2021**, *8*, 2002074.
[35] S. Neudeck, A. Mazilkin, C. Reitz, P. Hartmann, J. Janek, T. Brezesinski, *Sci. Rep.* **2019**, *9*, 5328.
[36] H. Y. Asl, A. Manthiram, *Science* **2020**, *369*, 140.
[37] H. Zheng, Q. Sun, G. Liu, X. Song, V. S. Battaglia, *J. Power Sources* **2012**, *207*, 134.
[38] K. Amine, Z. Chen, Z. Zhang, J. Liu, W. Lu, Y. Qin, J. Lu, L. Curtis, Y.-K. Sun, *J. Mater. Chem.* **2011**, *21*, 17754.
[39] S. Neudeck, F. Walther, T. Bergfeldt, C. Suchomski, M. Rohnke, P. Hartmann, J. Janek, T. Brezesinski, *ACS Appl. Mater. Interfaces* **2018**, *10*, 20487.
[40] R. Ramos, G. Cunge, B. Pelissier, O. Joubert, *Plasma Sources Sci. Technol.* **2007**, *16*, 711.
[41] J. Fu, A. Osaka, T. Nanba, Y. Miura, H. Yamanaka, *Mater. Lett.* **1992**, *15*, 264.
[42] L. de Biasi, A. Schiele, M. Roca-Ayats, G. Garcia, T. Brezesinski, P. Hartmann, J. Janek, *ChemSusChem* **2019**, *12*, 2240.
[43] A. Wuersig, W. Scheifele, P. Novák, *J. Electrochem. Soc.* **2007**, *154*, A449.
[44] J. K. Papp, N. Li, L. A. Kaufman, A. J. Naylor, R. Younesi, W. Tong, B. D. McCloskey, *Electrochim. Acta* **2021**, *368*, 137505.
[45] F. Strauss, J. H. Teo, A. Schiele, T. Bartsch, T. Hatsukade, P. Hartmann, J. Janek, T. Brezesinski, *ACS Appl. Mater. Interfaces* **2020**, *12*, 20462.
[46] T. Hatsukade, A. Schiele, P. Hartmann, T. Brezesinski, J. Janek, *ACS Appl. Mater. Interfaces* **2018**, *10*, 38892.
[47] J. Wandt, A. T. S. Freiberg, A. Ogrodnik, H. A. Gasteiger, *Mater. Today* **2018**, *21*, 825.
[48] R. Jung, M. Metzger, F. Maglia, C. Stinner, H. A. Gasteiger, *J. Phys. Chem. Lett.* **2017**, *8*, 4820.
[49] W. Zhang, Y. Liu, J. Wu, H. Shao, Y. Yang, *J. Electrochem. Soc.* **2019**, *166*, A863.
[50] E. Markevich, G. Salitra, M. Afri, J. Kulisch, P. Hartmann, D. Aurbach, *J. Electrochem. Soc.* **2019**, *166*, A1685.
[51] Y. Fan, J. Wang, Z. Tang, W. He, J. Zhang, *Electrochim. Acta* **2007**, *52*, 3870.
[52] Y. Suzuki, T. Park, K. Hachiya, T. Goto, *J. Fluorine Chem.* **2020**, *238*, 109616.
[53] A. Dreveton, *Procedia Eng.* **2012**, *46*, 255.
[54] A. Guéguen, D. Streich, M. He, M. Mendez, F. F. Chesneau, P. Novák, E. J. Berg, *J. Electrochem. Soc.* **2016**, *163*, A1095.
[55] S. Solchenbach, M. Metzger, M. Egawa, H. Beyer, H. A. Gasteiger, *J. Electrochem. Soc.* **2018**, *165*, A3022.
[56] J. Zhou, P. S. Fedkiw, *Electrochim. Acta* **2003**, *48*, 2571.
[57] J. Zhou, P. S. Fedkiw, S. A. Khan, *J. Electrochem. Soc.* **2002**, *149*, A1121.
[58] S. Jockusch, J. Sivaguru, N. J. Turro, V. Ramamurthy, *Photochem. Photobiol. Sci.* **2005**, *4*, 403.
[59] E. Boix-Garriga, B. Rodríguez-Amigo, O. Planas, S. Nonell, in *Singlet Oxygen: Applications in Biosciences and Nanosciences*, (Eds.: S. Nonell, C. Flors), Vol. *1*, The Royal Society of Chemistry, London **2016**, pp. 39.
[60] R. Jung, M. Metzger, F. Maglia, C. Stinner, H. A. Gasteiger, *J. Electrochem. Soc.* **2017**, *164*, A1361.
[61] R. Oesten, U. Heider, M. Schmidt, *Solid State Ionics* **2002**, *148*, 391.
[62] T. Ohzuku, A. Ueda, M. Nagayama, *J. Electrochem. Soc.* **1993**, *140*, 1862.
[63] C.-S. Kim, K. M. Jeong, K. Kim, C.-W. Yi, *Electrochim. Acta* **2015**, *155*, 431.
[64] K. Kleiner, P. Jakes, S. Scharner, V. Liebau, H. Ehrenberg, *J. Power Sources* **2016**, *317*, 25.
[65] B. B. Berkes, A. Jozwiuk, H. Sommer, T. Brezesinski, J. Janek, *Electrochem. Commun.* **2015**, *60*, 64.
[66] B. B. Berkes, A. Jozwiuk, M. Vracar, H. Sommer, T. Brezesinski, J. Janek, *Anal. Chem.* **2015**, *87*, 5878.
[67] K. L. Parry, A. G. Shard, R. D. Short, R. G. White, J. D. Whittle, A. Wright, *Surf. Interface Anal.* **2006**, *38*, 1497.
[68] J. H. Scofield, *J. Electron Spectrosc. Relat. Phenom.* **1976**, *8*, 129.
[69] S. Tanuma, C. J. Powell, D. R. Penn, *Surf. Interface Anal.* **1993**, *21*, 165.